EXPERIMENTAL CHARACTERIZATION OF STRAIGHT COMPOUND-CHANNEL TURBULENT FIELD

Ricardo Azevedo[1], Luis Rojas-Solórzano[2] & João Leal[1]

[1]CEHIDRO & Department of Civil Engineering, FCT, Universidade Nova de Lisboa, Portugal, Caparica 2829-516
[2]Department of Energy Conversion and Transport, Universidad Simón Bolívar, Venezuela, Sartenejas, Baruta, Edo. Miranda 89000
E-mail: ricardopereira84@gmail.com

Abstract

Straight compound-channel flows have been studied by many authors, mainly concerned with mean flow variables. Detailed information on the complex turbulent field of these flows is still scarce. In the present paper, high data rate measurements were obtained for the streamwise and vertical velocity components, using a 2D Laser Doppler Velocimeter in a experimental compound flume. The filtered velocities time series allowed the computation of relevant turbulence statistics: autocorrelation functions, dissipation spectra, turbulence scales and dissipation rate. The results are analyzed by comparison with universal laws drawn for isotropic turbulent 2D fully developed open-channel flow. The presence of strong secondary currents does not affect the universal law in the floodplain, as long as the constants are changed. In the main channel the 3D behavior of the flow is more pronounced and the universal laws fail to reproduce accurately the experimental results.

Introduction

Straight compound-channel flows have been studied by many authors due to their practical importance related to floods in rivers. In terms of physical interpretation and numerical modeling they constitute a challenge, since they present a complex 3D structure that can include large scale horizontal vortices and helicoidal longitudinal vortices, also known as secondary currents (Shiono & Knight 1991). Despite the presence of these structures, most studies are focused only in the mean flow variables. The studies of Knight & Shiono (1990), Shiono & Knight (1991), Tominaga & Nezu (1991), Nezu *et al.* (1999), Prooijen *et al*. (2005), Stocchino & Brocchini (2010) and Stocchino *et al*. (2011) are among the few studies where the turbulent field in straight compound-channel was addressed. Nevertheless, the influence of the vortex structure in the turbulent scales and in the dissipation rate was not assessed. In the present study, high data rate measurements were obtained for the streamwise and vertical velocity components, using a 2D Laser Doppler Velocimeter in an experimental compound flume with a deep flow, where secondary currents are dominant (*cf.* Nezu *et al.*, 1999). The analysis of the effect of secondary currents in the turbulent scales and in the dissipation rate is made by comparison with universal laws drawn for isotropic turbulent 2D fully developed open-channel flow (Nezu & Nakagawa, 1993).

Experimental Setup

The experiments were conducted in an asymmetric compound flume built in cement at University of Beira Interior. The flume is 11.60 m long and 0.790 m wide. The main channel width is 0.205 m, while the floodplain width is 0.540 m. The width of the region between the main channel and floodplain, called interface, is 0.054 m and the bank full depth is 0.051 m, as shown in Figure 1.

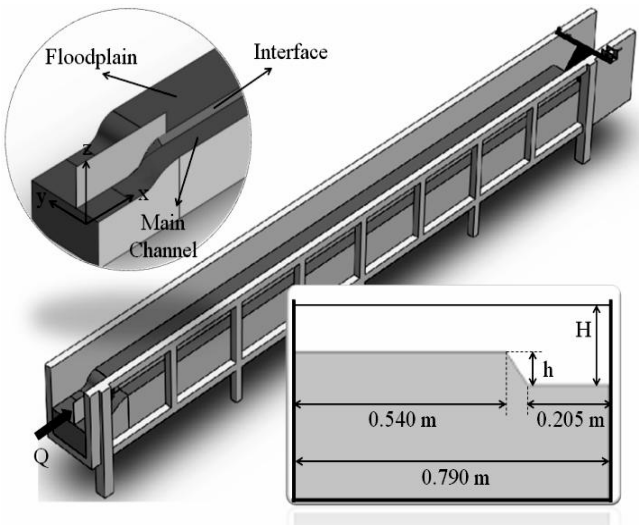

Figure 1: Description of the asymmetric compound flume.

The average longitudinal bottom slope of the main channel and floodplain is 0.986 and 0.911 mm/m, respectively. To set the quasi-uniform flow it was necessary to measure the water depth in the middle of the main channel and also in the floodplain to verify that the value of the free-surface

slope, in both sub-regions, was between the value of the main channel and the floodplain longitudinal bottom slope.

The measurements of the velocity field were made with a 2D Laser Doppler Velocimeter (LDV) in a cross-section located 9.0 m from the inlet of the channel, where the downstream gate does not influence the flow. Measurements in backscattering mode were performed through a glass window located on the main channel lateral wall of the channel next to the main channel. The total number of points measured to characterize the cross-section was 1,148. The measurement time was 210 s per point and aluminum oxide powder was used as seeding.

The discharge used during the experiments was 23.16 l/s and the quasi-uniform flow water depth was 0.1033 m. The relative water depth, H_r, calculated through the equation (1) was 0.50. In that equation H_{fp} and H_{mc} are the floodplain and main channel water depths, respectively.

$$H_r = H_{fp} / H_{mc} \quad (1)$$

Results and Discussion

The terms used to describe the velocity field are *u* and *w* for the instantaneous velocity; *u*' and *w*' for the velocity fluctuations; *U* and *W* for the time-averaged velocity; and *U*' and *W*' for the root mean square or turbulence intensity in the longitudinal direction, *X*, and vertical direction, *Z*, respectively (see Figure 1).

Table 1 shows the experimental conditions where measurements were made. The cross-section mean velocity, U_{cs}, was calculated by the relation between the inlet discharge and the area of the cross section. The geometrical method ($U_* = \sqrt{gR_hS_0}$, where $g = 9.8\ \mathrm{m/s^2}$ is the gravitational acceleration and R_h is the hydraulic radius) was used to compute the friction velocity of the section. Further, the Reynolds number and Froude number were calculated by the expression $Re = 4U_{cs}R_h/\nu$ (ν = 7.96x10^{-7} m^2/s is the kinematic viscosity of water at 30º C) and $Fr = U_{cs}/\sqrt{gH_{mc}}$, respectively.

Table 1: Experimental Conditions.

Q (l/s)	H_{mc} (m)	H_r	U_{cs} (m/s)	U_* (m/s)	Re (x10^{-4})	Fr
23.16	0.1033	0.50	0.4301	0.0227	11.78	0.425

Velocity Distribution

Figure 2 shows the time-averaged velocity distribution *U* and *W* measured in the cross section at 9.0 m from the inlet of the cannel, as well as turbulent intensity distribution *U*'/U_* and *W*'/U_*. The interaction between the main channel flow (with higher velocity and inertia) and floodplain flow (with lower velocity and inertia) generates a momentum transfer causing the formation of different types of turbulent structures as vertical axis vortex, due to the shear layer between the main channel and floodplain flows, or longitudinal axis vortex, called secondary currents, due to the anisotropy of turbulence (Shiono & Knight, 1991, Nezu *et al*., 1999).

In Figure 2a, an ascendant flow in the interface region near the upper interface is evident, as well as the descendant flow in the floodplain region near the interface (0.26 m ≤ *Y* ≤ 0.29 m) and in the main channel region near the lower interface. The generation of the ascendant/descendant flow (secondary currents) is caused by the strong anisotropy between the floodplain and main channel flows, resulting in a vortex on the interface/floodplain region, called "floodplain vortex", and a vortex in the main channel/interface region called "main channel vortex" (*cf*. Tominaga & Nezu, 1991).

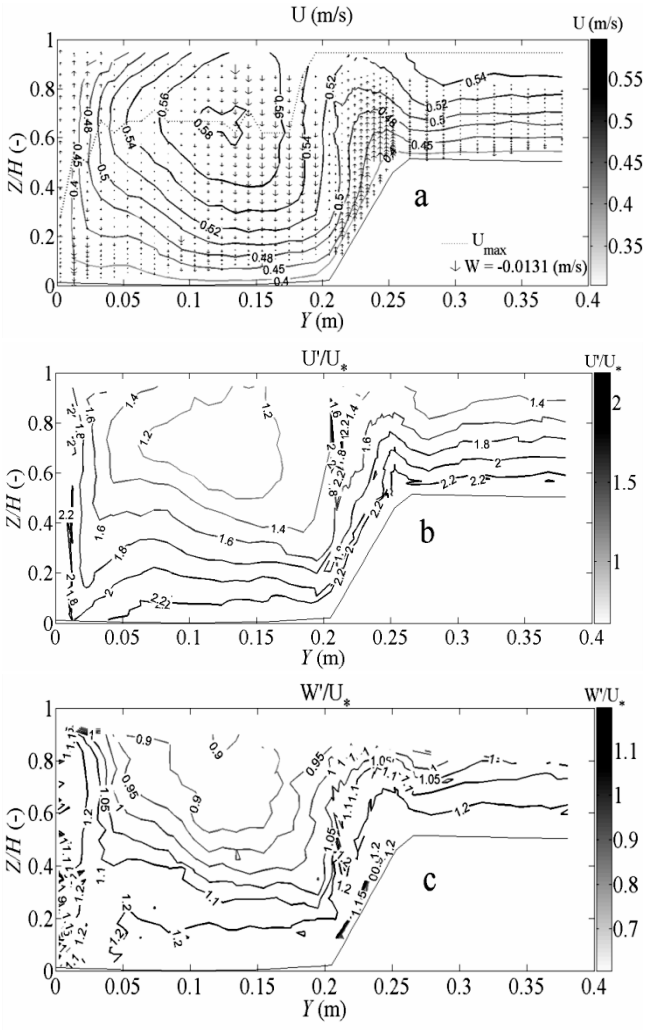

Figure 2: (a) Isovels of mean velocity *U* and vectors of mean velocity *W*; (b) Isovels of turbulent intensity *U*'; (c) Isovels of turbulent intensity *W*'.

The magnitude of *W* velocity in the main channel and interface region is similar, around 30% of U_*. In the floodplain region near the interface, the magnitude of the *W* velocity decreases until approximately 10% of U_*. The strong descendant flow in the main channel region is due to the meeting of two vortexes, the "main channel vortex" and the "free-surface vortex", that is caused by the anisotropy of lateral wall and free-surface turbulence (Nezu & Nakagawa, 1993). On the other hand, Figure 2a shows how the isovels are affected by the momentum transport of the secondary currents. Since there is an ascendant flow in the interface region, the *U* isovels are displaced upwards by influence of the *W* velocity. The same effect occurs with the descendant flows. Further, due to effects of the "free-surface vortex", the maximum *U* velocity is in the middle of the main channel at 65% of the water depth.

For the *U*' turbulent intensity (Figure 2b) a similarity with the isovels of *U* is observed. However, the bulging of the isovels *U*' is more intense and corresponds with the ascendant/descendant flows of the cross section. On the other hand, the lower turbulent intensity *U*' is observed in the middle of the main channel below the free-surface due to the dip-velocity phenomenon. In the case of the turbulent intensity *W*' (Figure 2c), a bulging of the isovels in the upper interface is again observed. The main difference between *U*' and *W*' is that, while the lower turbulent intensity *U*' is below the free-surface, the *W*' turbulent intensity decreases towards the free-surface. Further, the magnitude of *W*' is slightly smaller than the magnitude of *U*'.

Figure 3 shows the vertical distribution of U^+ for Y = 0.104 m, 0.205 m, 0.253 m and 0.380 m, with U^+ and Z^+ defined as:

$$U^+ = U/U_{*(Y)} \tag{2}$$

$$Z^+ = ZU_{*(Y)}/\nu \tag{3}$$

where the term $U_{*(Y)}$ is the local friction velocity. The local friction velocity was determined using the log-law, considering that the vertical location of the measured point could have some uncertainties. Therefore, a displacement ΔZ was considered in the vertical location. The ΔZ was adjusted so that the integral constant of the log-law (equation 4, where κ = 0.41 is the von Kármán constant) was equal to A = 5.3, valid for 2D open-channel flow (*e.g.* Nezu & Nakagawa, 1993). The log-law is presented in Figure 3 by a line.

$$U^+ = \frac{1}{\kappa}\ln\left[\frac{(Z+\Delta Z)U_{*(Y)}}{\nu}\right] + A \tag{4}$$

The velocity profiles in the upper interface and floodplain present a trend similar to 2D open-channel flows, i.e. they follow the log-law in the inner layer and as they approach the free-surface they depart from the log-law to a log-wake law (*cf.* Nezu & Nakagawa, 1993). In the main channel and lower interface the velocity profiles also follow the log-law, but they decrease abruptly near the free-surface, which is due to the presence of strong secondary currents.

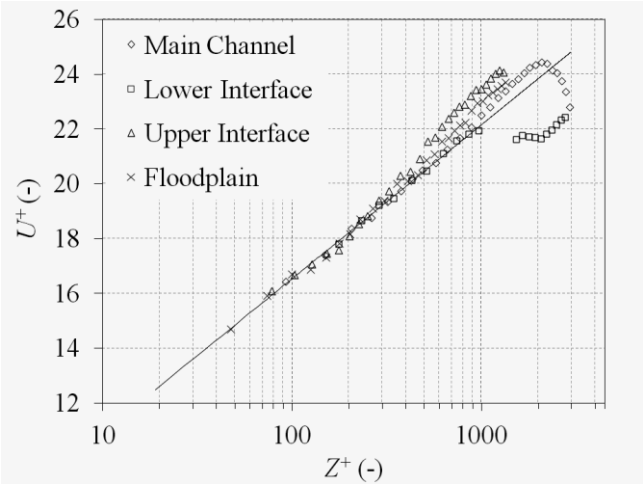

Figure 3: Vertical distribution of time-averaged velocity *U*.

Figure 4 shows the distribution of turbulent intensity U' against Z/H. In the figure is also included the universal equation (5) valid for the intermediate region ($0.1 < Z/H < 0.6$) of 2D fully developed flows (*e.g.* Nezu & Nakagawa, 1993).

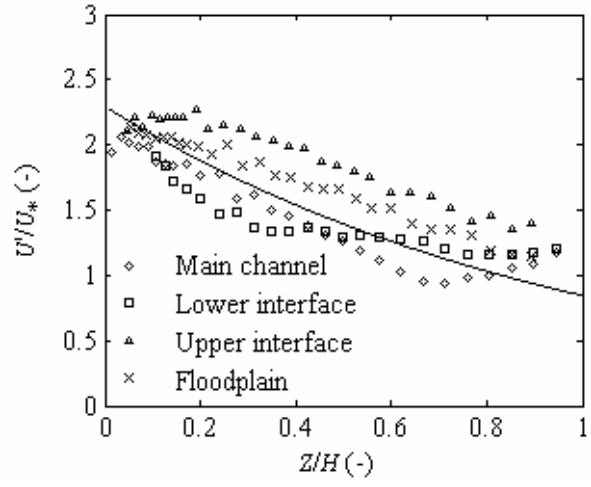

Figure 4: Vertical distribution of turbulent intensity *U*'.

$$U'/U_* = 2.30\exp(-Z/H) \quad (5)$$

The experimental results for the upper interface and floodplain seem to follow a similar trend to equation (5), although with higher turbulent intensities. This means that the flow at those two verticals behaves like a 2D flow but with higher turbulence intensity. In the main channel the experimental data follows the universal equation until *Z*/*H* around 0.6. As the flow approaches the free surface the turbulent intensity starts to increase, which is due to the presence of strong secondary currents. For the lower interface, until *Z*/*H* around 0.3, the turbulent intensity decreases and stays below the universal equation. For *Z*/*H* >0.3 the turbulent intensity reaches a plateau. The discrepancies between the experimental results and the universal equation (5) clearly highlight the 3D character of the flow.

Turbulent longitudinal scales and dissipation

The velocities time series can be transformed into an equally spaced temporal record by taking an averaged time step, τ:

$$\tau = t_{\max}/n \quad (6)$$

being $t_{\max}$ the maximum time in the record and n the number of measurements in the record. The instantaneous velocity values for each time can be obtained from the original record through linear regression. Adopting Taylor's frozen-field hypothesis, the time record can be transformed into a space record, using a convection velocity, U_c, with a space interval

$$r = U_c\tau \quad (7)$$

In the present study, for each record, U_c was considered constant and equal to the time-averaged velocity *U*. Although this criterion implies that the convection velocity is the same for all flow scales, which is not true for most cases, it holds for large and intermediate scales if turbulent intensity is less than 20% (*e.g*. Tropea *et al*., 2007). The space record allows the computation of the longitudinal autocorrelation function (*e.g*. Pope, 2000)

$$\rho(r) = \frac{\overline{u'(r)u'(x+r)}}{\overline{u'^2}} \quad (8)$$

One example of autocorrelation function is presented in Figure 5 for the point *Z*/*H* = 0.46 in the main channel vertical. In the figure, the integral length scale obtained by equation (9) (*e.g*. Pope, 2000) is also presented

$$L_x = \int_0^\infty \rho(r)\,dr \quad (9)$$

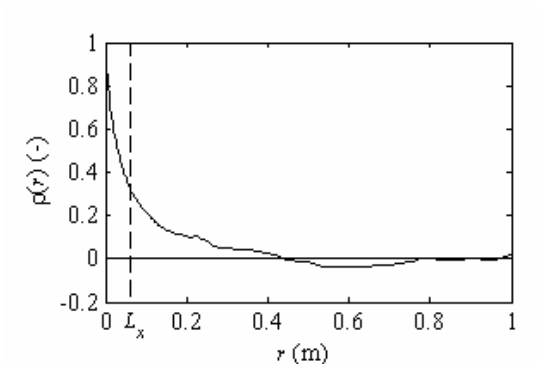

Figure 5: Longitudinal autocorrelation function.

Figure 6 shows the vertical distribution of the longitudinal integral scales obtained from the autocorrelation function for all points. In the figure, equation (10) is also plotted with B_1 = 1.0, 1.5, 2.5 and 3.5. This equation was proposed by Nezu & Nakagawa (1993) for 2D fully developed open-channel flow, with B_1 approximately equal to 1.0.

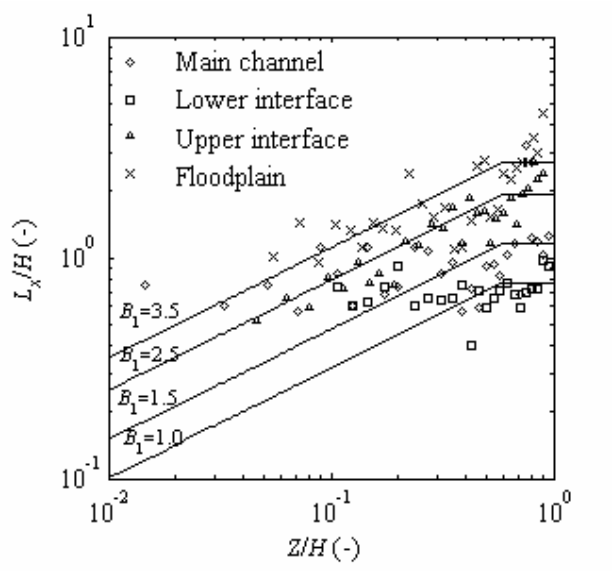

Figure 6: Vertical distribution of the longitudinal integral length scale, L_x.

$$\frac{L_x}{H} = \begin{cases} B_1 (Z/H)^{1/2} & \text{for } Z/H < 0.6 \\ 0.77 B_1 & \text{for } Z/H > 0.6 \end{cases} \quad (10)$$

The upper interface and the floodplain results fairly follow equation (10), but with higher coefficient B_1. Near the free surface, contrary to equation (10), the experimental data do not present a plateau, instead the integral length scale continue to increase towards the free-surface. For the main channel vertical the integral length scale is almost constant through the depth, with a value close to the flow depth. This indicates that the secondary current in the main channel dictates the characteristic size of the large turbulent structures. The lower interface present a similar pattern of the one observed for the main channel, but with smaller integral scale.

In Figure 7 the longitudinal dissipation spectrum is presented for point Z/H = 0.8 in the lower interface. The spectrum was obtained using a Yule-Walker spectral estimator which is extremely smooth (*e.g.* Stoica & Moses, 2005), but allows an easy identification of the inertial subrange. The dissipation spectrum can be computed from the velocity power spectrum, E_{11}, using the Kolmogorov $-5/3$ law for the inertial subrange (e.g. Pope, 2000)

$$E_{11} = C_1 k_w^{-5/3} \varepsilon^{2/3} \Rightarrow \varepsilon = \left(E_{11} \Big/ \left(C_1 k_w^{-5/3} \right) \right)^{3/2} \quad (11)$$

where ε is the turbulent dissipation rate, k_w is the wave number and C_1 is a universal constant equal to ≈0.53. In the figure the dissipation rate, ε, was taken from the plateau and the integral scale, L_x, and the microscale, λ_x, are also presented.

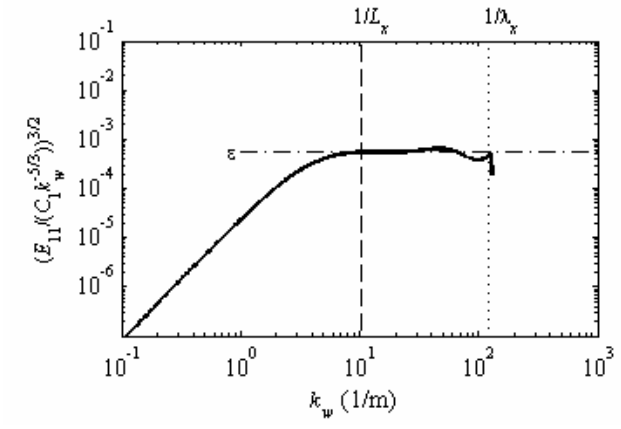

Figure 7: Longitudinal dissipation spectrum for point Z/H = 0.8 in the lower interface.

The microscale was obtained from the dissipation rate by assuming isotropic turbulence (*e.g.* Tropea et al., 2007)

$$\lambda_x = \sqrt{\frac{30 \nu U'^2}{\varepsilon}} \quad (12)$$

Figure 8 shows the vertical distribution of the longitudinal microscale for all points. In the figure is also plotted the semi-theoretical relation proposed by Nezu & Nakagawa (1993) for 2D fully developed open-channel flow

$$\frac{\lambda_x}{H} = \sqrt{\frac{15 B_1}{2.3 K Re_*}} \left(\frac{Z}{H} \right)^{1/4} \exp\left(\frac{Z}{2H} \right) \quad (13)$$

where

$$Re_* = U_* H / \nu \quad (14)$$

$$K = 0.691 + 3.98 \Big/ \sqrt{Re_L} \quad (15)$$

$$Re_L = U' L_x / \nu \quad (16)$$

In equations (13) to (16) L_x is computed using equation (10) and U' using equation (5).

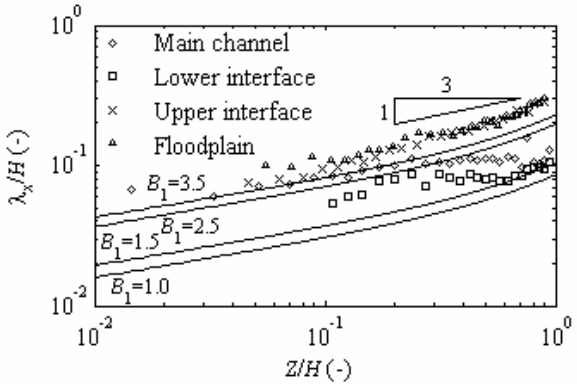

Figure 8: Vertical distribution of the longitudinal microscale, λ_x.

The results of the microscale for the floodplain and the upper interface are almost coincident and present a similar trend to the theoretical curves. The experimental values are higher than the theoretical ones, which can be attributed to the underestimation of U' values given by equation (5) (see Figure 6). For the main channel and lower interface the

experimental results depart from the theoretical curves, mostly due to the wrong estimation of *U*' caused by the influence of strong secondary currents.

Figure 9 shows the vertical distribution of the dissipation rate for all points, computed through the dissipation spectra as mentioned before (see Figure 7). In the figure, the equation proposed by Nezu & Nakagawa (1993) for 2D fully developed open-channel flows is included

$$\frac{\varepsilon H}{U_*^3} = \frac{12.2K}{B_1}\left(\frac{Z}{H}\right)^{-1/2}\exp\left(-\frac{3Z}{H}\right) \qquad (17)$$

The experimental results show good agreement with the theoretical curves, except for the lower interface where the dissipation is substantially higher for the free-surface region. The extra dissipation must be linked to the strong secondary currents observed.

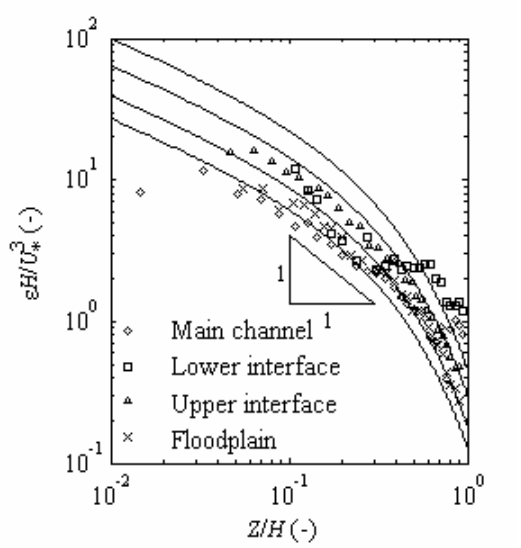

Figure 9: Vertical distribution of the dissipation rate, ε.

Conclusions

For deep water flow in straight compound channel the results presented above allow to extract the following conclusions:

- The universal laws for 2D fully developed open-channel flows are valid in the upper interface and floodplain, although the coefficients have to be increase, mostly due to the increase of turbulent intensity. This should be a consequence of the shallowness of the flow which contributes to maintain boundary turbulence as the dominant process.
- For the lower interface and main channel, the presence of strong secondary currents contributes to the non validity of the universal laws, even if their coefficients are changed. This means that the 3D character of the flow is "printed" in the turbulent field and boundary turbulence should not be dominant.

Acknowledgements

The authors acknowledge University of Beira Interior for allowing the realization of the experiments. The authors wish to acknowledge the financial support of the Portuguese Foundation for Science and Technology through the project PTDC/ECM/70652/2006. The first author wishes to acknowledge the financial support of the Portuguese Foundation for Science and Technology through the Grant SFRH/BD/33646/2009. A special acknowledgment is due to Prof. Rui Ferreira for his support on the computation of turbulent quantities.

References

Knight, D., & Shiono, K. (1990). Turbulence measurements in a shear layer region of a compound channel. *Journal of Hydraulic Research*, 28(2), pp. 175-196.

Nezu, I., Onitsuka, K., & Iketani, K. (1999). Coherent horizontal vortices in compound open channel flow. *Hydraulic Modeling*, eds. V.P. Singh, I.W. Seo, & J.H. Sonu, Water Resources Publications, pp. 17-32.

Nezu, I., & Nakagawa, H. (1993). *Turbulence in open-channel flows*. IAHR Monograph Series, A.A. Balkema, Rotterdam, Netherlands.

Pope, S.B. (2000). *Turbulent Flows*. 1st edition, Cambridge University Press.

Prooijen, B., Battjes, J., & Uijttewaal, W. (2005). Momentum Exchange in straight uniform compound channel flow. *Journal of Hydraulic Engineering*, 131(3), pp. 175-183.

Shiono, K., & Knight, D.W. (1991). Turbulent open-channel flows with variable depth across the channel, *Journal of Fluid Mechanics*, 222, pp. 617-646.

Stocchino, A., Besio, G., Angiolani, S., & Brocchini, M. (2011). Lagrangian mixing in straight compound channels. *Journal of Fluid Mechanics*, 675, pp. 168-198.

Stocchino, A., & Brocchini, M. (2010). Horizontal mixing of quasi-uniform, straight, compound channel flows. *Journal of Fluid Mechanics*, 643, pp. 425-435.

Stoica, P., & Moses, R.L. (2005). *Spectral analysis of signals*. 1st edition, Prentice Hall.

Tominaga, A., & Nezu, I. (1991). Turbulent structure in compound open channel flows. *Journal of Hydraulic Engineering*, 117(1), pp. 21-40.

Tropea, C., Yarin, A.L., & Foss, J.F. (2007). *Springer Handbook of Experimental Fluid Mechanics*. 1st edition, Springer.